Growth and structure in abalone shell

Albert Lin, Marc André Meyers*

*Department of Mechanical and Aerospace Engineering, University of California,
San Diego, La Jolla, CA 92093-0411, USA*

Abstract

The growth and self-assembly of aragonitic calcium carbonate found in the shell of abalone (Haliotis) is described. This was accomplished through the close examination of laboratory-grown flat pearl samples and cross-sectional slices of the nacreous shell. Further understanding of the sequenced assembly has been obtained. It has been confirmed that the growth of the aragonite component of the composite occurs by the successive nucleation of aragonite crystals and their arrest by means of a protein-mediated mechanism; it takes place in the "Christmas-tree pattern" [Nature 49 (1994) 371]. It is shown that the protein layer is virtually absent where plates on a same plane abut (along lateral surfaces of tiles). This suggests a mechanism of c-axis aragonite growth arrest by the deposition of a protein layer of approximately 20–30 nm that is periodically activated and determines the thickness of the aragonite platelets, which are remarkably constant (0.5 μm). This platelet size was measured for animals with shell diameters of 10, 50, and 200 mm and was found to be constant. The overall growth process is expressed in terms of parameters incorporating the anisotropy of growth velocity in aragonite (V_c, the velocity along c axis, and V_{ab}, the velocity in basal plane). Comparison of laboratory-raised and naturally-grown abalone indicates growth regulated by the level of proteinaceous saturation. Naturally-grown abalone exhibits mesolayers (growth bands) ∼0.3 mm apart; it is proposed that they result from seasonal interruptions in feeding patterns, creating thicker (∼10–20 μm) layers of protein. These mesolayers play a critical role in the mechanical properties, and are powerful crack deflectors. The viscoplastic deformation of the organic inter-tile layers is responsible for the significant improvement of tensile strength over the tensile strength of monolithic aragonite.
© 2004 Elsevier B.V. All rights reserved.

Keywords: Biological materials; Abalone; Mechanical properties; Biomimetics; Abalone

1. Introduction

The study of materials that have evolved through millions of years of evolution and natural selection can provide insights into heretofore-unexploited mechanisms of toughening. *Biomimetics* is an interdisciplinary area between Materials Science and Biology in which lessons learned from biology form the basis for novel material concepts [2,3]. This area investigates biological structures, establishing relationships between properties and structures in order to develop methods of processing and microstructural design for new materials. Sarikaya [2] divides the field into:

(a) *Biomimicking:* the understanding of these biological systems and application of concepts to synthetic materials using current technology.
(b) *Bioduplication:* a more advanced stage, in which new methodologies, such as genetic engineering, will be used to produce an entire class of new materials.

Biological organisms produce complex composites that are hierarchically organized in composition and microstructure, containing both inorganic and organic components in complicated mixtures. These organism-controlled materials are synthesized at ambient temperature and atmospheric conditions. The unique microstructures and associated properties in biological composites are stimulating creativity in the development of future synthetic materials. There are numerous examples of biomaterials with unique mechanical properties [4–7]: silk, antler, hedgehog spines [8], silica rods in

---

* Corresponding author. Tel.: +1 619 534 4719; fax: +1 619 534 5698.
E-mail address: mameyers@ucsd.edu (M.A. Meyers).

sea sponges (possessing three times the flexural strength of monolithic/synthetic silica [9]), pink conch [10] (*Strombus gigas*), abalone [2,11,12] (*Haliotis*), and *Conus* [13,14].

These ceramic structures self-assemble and form nano-scale, hierarchical, composites that possess truly remarkable properties. Self-assembly is one of the manifestations of self-organization. Self-assembly is a concept that has received considerable attention in this respect [15–17].

Biomineralization involves the selective identification and uptake of elements and ionic molecules from the local environment and their incorporation into functional structures under strict biological mediation and control [18–21]. It is an important field of science and directly impacts Materials Science of the future, especially in regards to the creation of ceramic nano-structures by self-assembly.

The study whose results are reported herein had as primary objective the elucidation of the structure of the nacreous component of abalone shells. It represents the continuation of an earlier study focused on mechanical properties [22–24]. It is felt that the detailed knowledge of the structure is essential for a full understanding of the mechanical response. In particular, the role played by the organic component needs to be quantitatively understood and characterized.

2. Experimental methods

A 150 gal tank with chilled salt water (∼16 °C) was set up in the laboratory. Both red (*Haliotis rufescen*s) and green (*Haliotis fulgens*) abalone were transported from the open water facility (Marine Bioculture, Leucadia, CA) to the laboratory and subjected to experiments. The abalone were fed feather boa kelp (*Egregia menziesii*) and giant kelp *(Macrocystis pyrifera)* on a regulated schedule.

The "flat pearl" method pioneered by the UC Santa Barbara group [1] was used for growing the layers and subsequent extraction of nacre samples for observation. Glass slides 15 mm in diameter and TEM grids (nickel grid with Formvar coating) 3 mm in diameter were glued (only one spot using 5 min epoxy) to the growth surface of the shells. This surface was exposed by gently pushing back the mantle layer in the inside of the shell using a flat stainless steel scalpel with rounded, dull edges. No copper was used in the process because of the negative reaction of the animal. It was observed that the retracted mantle, exposing the extrapallial space, took a few days to relax back to its original position covering the glass slides. The growth was monitored by extracting glass slides and TEM grids after three separate periods of embedment: 7, 14, and 24 days. The numbers that will be quoted here will be 3, 10, and 20 days (a 4-day adjustment period having been subtracted. It takes a few days for the mantle to reposition itself over the glass slide. Hence, the numbers above should be corrected for this time, which is typically 2–4 days. An environmental SEM (FEI) at Scripps Institute of Oceanography (SIO) was used for characterization with accelerating voltages of 15–20 kV. Observation slides were examined immediately after removal in order to maintain hydration of the organic matrix. Before examination each slide was washed in purified water to remove salt build up (*Note*: it was observed that the coloration of slides after prolonged SEM observation changed from translucent to transparent).

Cross sectional samples of nacre were prepared from shells varying in length from 10 to 50 mm (*Haliotis fulgens*) and finally 200 mm (*Haliotis rufescens*). These shells were fractured and mounted on SEM sample holders. Samples were then coated with a thin film of gold using a gold sputtering machine. Some of the cross sectional samples were polished before examination, however, many were examined along the natural fracture surface.

In order to study the growth characteristics of nacre under varying feeding and environmental characteristics, a selected number of animals were subjected to starvation for certain periods of time. Specimens from this group were removed from the holding tank for a period of less then an hour before SEM examination. This sample was observed along the cross-section as well as growth surface. The results are reported in Section 4.

3. Structure

Jackson et al. [25] were among the first to determine the mechanical properties of nacre (in the bivalve *Pinctata umbricata*). They report a Young's modulus of approximately 70 GPa for dry and 60 GPa for wet samples; the tensile strength of nacre was found to be 170 MPa for dry and 140 MPa for wet samples. The work of fracture varied from 350 to 1240 J/m^2, depending on the span-to-depth ratio and the degree of hydration, wet nacre showing superior toughness by associated introduction of plastic work. In contrast, monolithic CaCO$_3$ showed a work of fracture that was about 3000 times less than that of the composite nacre material. Sarikaya et al. [2,11,12] conducted mechanical tests on red abalone. A fracture strength of 185 ± 20 MPa (in bending tests) and a fracture toughness of 8 ± 3 MPam$^{1/2}$ were obtained. The toughness of monolithic aragonite is approximately 1 MPam$^{1/2}$. This represents an eight-fold increase in the abalone shell and is in contrast with the large number (3000) obtained by Jackson et al.; this difference is due to the incorporation of the failure region [25]. Wet nacre fails "gracefully" and the energy absorption is considerable. Nevertheless, this is not incorporated into a "fracture toughness" calculation; the first drop in load determines the toughness. Menig et al. [22] found significant scatter in the compressive strength of abalone and successfully fit the distribution into a Weibull equation [26], obtaining a coefficient m consistent with synthetic ceramics ($m = 3.5–5.1$). They assessed that one of the basic differences between monolithic and laminated aragonite is the ratio between compressive and tensile strength: in nacre it is 1.5–3, being equal to 10–15 for monolithic aragonite. The compressive strength was in the 500–700 MPa range, whereas the tensile strength was

consistent with measurements by Jackson et al. [25] and Sarikaya [2], 180 MPa. Menig et al. [22] identified a mechanism for failure previously only seen in synthetic composites: microplastic buckling (kinking). This is analogous to the mechanism previously identified and investigated in composites [27–31]. The growth bands (mesolayers) played an important role. Evans et al. [32] and Wang et al. [33] have recently carried out an investigation into the tensile deformation of abalone and concluded that nano-asperities on the aragonite tiles are responsible for the mechanical strength. These nano-asperities create frictional resistance to sliding, in a manner analogous to fibers in composite material. They developed a mechanism that predicts the tensile mechanical response. It can be concluded from the above that the structure and its linkage to mechanical properties is not yet completely understood. In particular, the role played by the organic layer is not quantitatively understood.

The structure of *nacre* within the shells of abalone that we are studying, as well as other marine animals, is composed of a "brick-like" tiled structure of crystalline aragonite (an orthorhombic polymorph of $CaCO_3$); moreover there is a very high degree of crystallographic texture characterized by a nearly perfect "*c*-axis" alignment normal to the plane of the tiles. Aragonite is metastable at low pressures (lower than 0.4 GPa) and forms orthorhombic crystals that are often twinned and pseudo-hexagonal in cross-section. Sarikaya [2] observed this twinning by TEM and classified it into first-generation and second-generation twins. Three morphologies of the aragonite polymorph are observed in the abalone shell: tiles, block-like, and spherulitic. The two forms of $CaCO_3$, calcite (rhombohedral) and aragonite (orthorhombic), constitute the inorganic component of this ceramic/organic composite (95 wt.% ceramic, 5 wt.% organic material). The general structure of the shell is depicted in Fig. 1, which is adapted from Zaremba et al. [34]. Both the external layer (prismatic calcite) and the internal region (aragonite) are shown. The mantle epithelium of the abalone is responsible for secreting the chemicals that produce growth. It ejects them into the extrapallial space. Small terraced cones are shown on the growth surface. They correspond to the "Christmas trees" reported by Fritz et al. [1] and Zaremba et al. [34]. They will be discussed in Section 4.

Fig. 2(a) shows the structure of the nacre region at low magnification and Fig. 2(b) shows an electron micrograph of the layered structure. Two types of structure are seen in Fig. 2. The thicker layers (mesolayers, or heterolayers [34]) are approximately 300 μm thick and are separated by layers of viscoplastic material with a thickness of about 20 μm (Fig. 2(a)). The darker bands are thick protein layers that separate the mesolayers. These mesolayers were identified by Menig et al. [22] but are not often mentioned in other reports dealing with the mechanical properties of abalone. It should be noticed that these mesolayers were absent in green abalone raised domestically by Dr. David Leighton. It is thought that these thick organic layers form in abalone grown in the sea during periods in which there is little calcification. At a smaller scale the aragonite is comprised of tiles approximately 0.5 μm thick (Fig. 2(b)). These tiles are separated by thin organic layers acting as a viscoplastic glue (e.g. [22]). Fig. 2(c) shows a cross-section of partially demineralized nacre. The rigid "fins" correspond to the heterolayers (or mesolayers). They are much more rigid, by virtue of their thickness, than the nano-layers (organic layers between tiles). The latter are crumpled up between the mesolayers.

Fig. 3(a) shows a schematic drawing of tile stacking. They form an arrangement that may be represented by hexagons; sequential layers are not stacked exactly on top of each other, providing overlap between tiles which enhances the mechanical strength. Fig. 3(b) shows the inner surface of a small (10 mm) shell where growth had been interrupted. The tiles are clearly seen. Four different layers can be resolved in this SEM micrograph. The tiles have in general six faces, with a diameter of approximately 10 μm.

The effort by Belcher and coworkers represents the most comprehensive effort at understanding the structure and growth of abalone [34–40]. Shell growth begins with the secretion of proteins that mediate the initial precipitation of calcite, followed by a phase transition from calcite to the aragonite. Prismatic calcite is composed as columnar, crystallographically textured, crystals of rhombohedral calcite. There are at least seven proteins involved in the process. Recent results by Su et al. [41] have identified the block-like structure occurring at growth bands as aragonitic, and not calcitic, as previously thought [34–40]. The mesolayers (growth bands) correspond to periods of periodic growth arrest. This is discussed in Section 4. Fig. 4(a) shows two dark layers (SEM, backscattered) of organic material. The inside of the shell is in the bottom. The upper surface of the organic layer
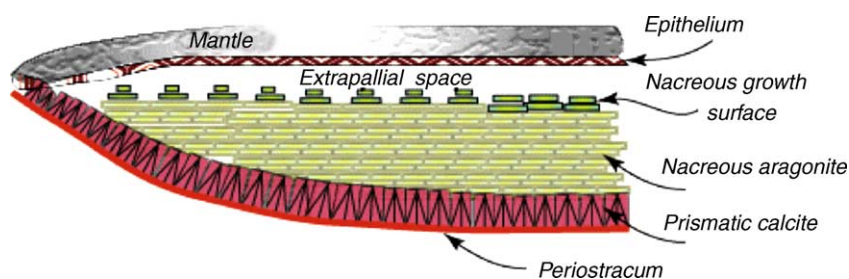

Fig. 1. Structure of typical mollusk shell (adapted from Zaremba et al. [34]).
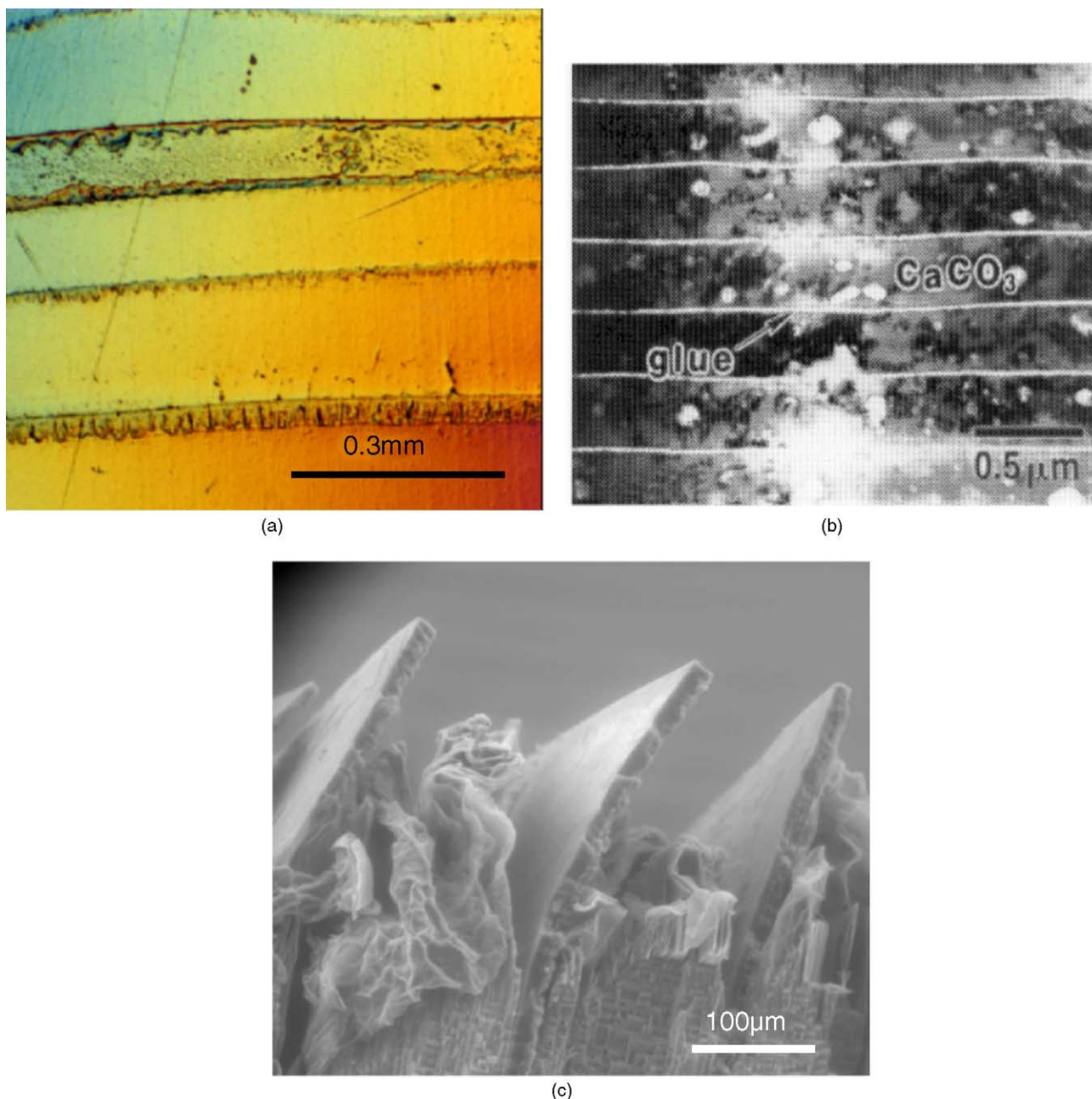
(a)

(b)

(c)

Fig. 2. Sections normal to abalone shell surface showing nacreous layer: (a) optical micrograph showing mesostructure with 0.3 mm layers separated by 20 µm protein layers; (b) TEM showing microstructure of tiles (from Menig et al. [22]); (c) partially demineralized specimen showing mesolayers (rigid "fins") and nano-layers (crumbled sheets) of organic material.

is smooth, while its lower surface is irregular. When biomineralization sets in again, it proceeds through the spherulitic morphology. After a certain time, tiled aragonite growth is reinitiated. The interfaces shown in Fig. 4(a) have been identified as regions where protein secretion has triggered the formation of a spherulitic layer upon which subsequent organic precipitation leads to the reformation of tiled aragonite. These results confirm the identification by Zaremba et al. [34] of a green organic/calcite heterolayer (Fig. 1, [34]). Zaremba et al. [34] report an organic layer with 5–15 µm thickness, consistent with Fig. 4(a). It should be noticed that more re-

cent X-ray diffraction by Su et al. [41] identifies the block-like and spherulitic morphologies observed at growth bands as orthorhombic (aragonitic). Fig. 4(b) shows the mesostructure of a specimen subjected to flexure. The powerful crack-deflection ability of the mesolayers is evident. Indeed, the mesolayers are more effective than the individual tiles in slowing the progression of crack.

The identification of the proteins involved has only been partially done to this date, although there is work to draw upon that has succeeded in extracting protein from shells (*Mytilus californanus*) and causing precipitation from supersaturated
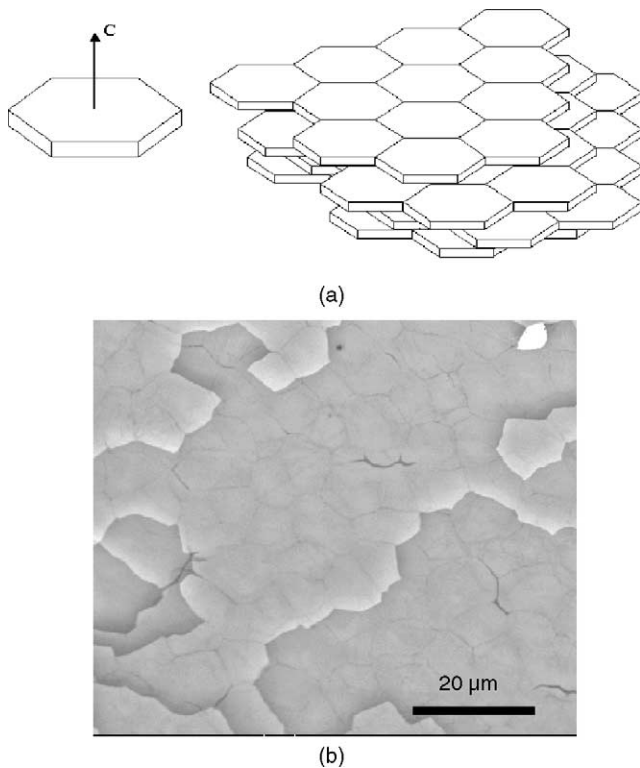
(a)

(b)

Fig. 3. (a) Schematic representation of stacked layers of aragonite tiles; (b) arrangement of tiles on inner surface of 10 mm shell; back-scattered image (SEM).

solutions of Ca^{2+} and CO_3^{2-} [46]. The crystal growth was carried out in vitro. This work indeed provides a valuable database for this study. In particular, Shen et al. [37] have reported the characterization of the cDNA coding for "Lustrin A" which is a protein they have identified within the nacreous layer of *Haliotis rufescens*. Nakahara et al. [42] and Sarikaya [2] describe the organic phase as having a sandwich form. The center region is structurally more rigid with high chitin content. Aspartic acid is a major constituent of the acid soluble components. Other constituents are glutamic acid, serine, glycine, alanine. The TEM photographs of Sarikaya [2] show clearly that the organic layer is composed of at least one central "scaffold" layer that has been called a beta sheet. Weiner and coworkers [43–47] describe this beta sheet and propose that an aspartic acid rich protein $(Asp–Y)_n$, where Y is an amino acid, bonds to the Ca^{2+} ions of the aragonite structure. References to similar mechanisms date back to 1980 [45]. Addadi and Weiner [46] describe the phenomenon of stereoselectivity in considerable detail and provide three possible explanations for it:

(a) The aspartic acid-rich protein that they used for in vitro experiments binds to calcium atoms preferentially. Indeed the $(0\,0\,1)$ plane of aragonite is characterized by protruding calcium atoms, as shown in Fig. 5(a). The $(0\,0\,1)$ plane is the top surface. The calcium atoms are black; the carbon atoms are black and smaller; the oxygen atoms are gray.

(b) The relative position of calcium and carbonate ions creating a favorable electric charge on the $(0\,0\,1)$ face for the adsorption of protein.

(c) Carboxylate groups (CO_3^-) are oriented perpendicular to the $(0\,0\,1)$ face and therefore complete the coordination around the protein-bound calcium atoms.

Based on this, it is herein proposed that the aspartic acid-rich protein attaches itself preferentially to the $(0\,0\,1)$ plane of the aragonite. This happens periodically by an organism-mediated mechanism. Fig. 5(b) shows the unit cell and the aspartic-acid rich protein $(Asp–Y)_n$ attaching itself to the Ca^{2+} ions. These proteins, on their turn, attach themselves to the more rigid beta sheet. In this manner, an organic layer structure consistent with Sarikaya's [2] observations is produced. This explanation is consistent with the growth mechanism discussed in Section 4.

4. Growth

4.1. Observations on "flat pearl" specimens

The structures created during growth were observed using the "flat pearl" method introduced by Fritz et al. [1]. After 3 days (Fig. 6), one can see the beginning of the formation of an organic layer. This proteinaceous layer has been observed by Zaremba et al. [34], Shen et al. [37], and Fritz and Morse [40]. After 10 days, this layer has grown substantially, and is almost continuous (Fig. 7). In a few regions, one sees the onset of growth of another phase on this layer. This is thought to correspond to the onset of biomineralization. This layer is also related to the beta sheet conformation postulated by Addadi et al. [44]. In Figs. 6 and 7, a 3 mm TEM specimen grid was used. The nucleation seems to be aided by irregularities along the grid.

After 20 days, one finds an entirely different structure. Fig. 8(a) shows a low magnification view, and it is seen that the mineral phase nucleates randomly over the proteinaceous layer. A closer observation, shown in Fig. 8(b) reveals the "Christmas tree" pattern described earlier by Fritz et al. [1], Shen et al. [37], and Fritz and Morse [40]. However, it should be noted that the center-to-center distance is less than the tile size in natural abalone, which is $10 \mu m$. It is speculated that the glass provides a greater areal density of nucleation sites. The density of sites in Fig. 8(a) was measured and is equal to 0.06 sites/μm^2 (517 sites in entire photomicrograph). From this, one obtains, in a manner analogous to dislocation density (inverse of square root of density), a center-to-center distance of $4.04 \mu m$. A regular pattern of tiles with $10 \mu m$ (that is observed in shell sections) will give a site density of 0.01 sites/μm^2. Thus, there are six times as many sites on the glass slip than the steady state value. It is speculated that the areal density of "Christmas trees" has not yet reached the steady state. Indeed one observes a smaller terraced cone being absorbed by surrounding larger ones in Fig. 8(b). There
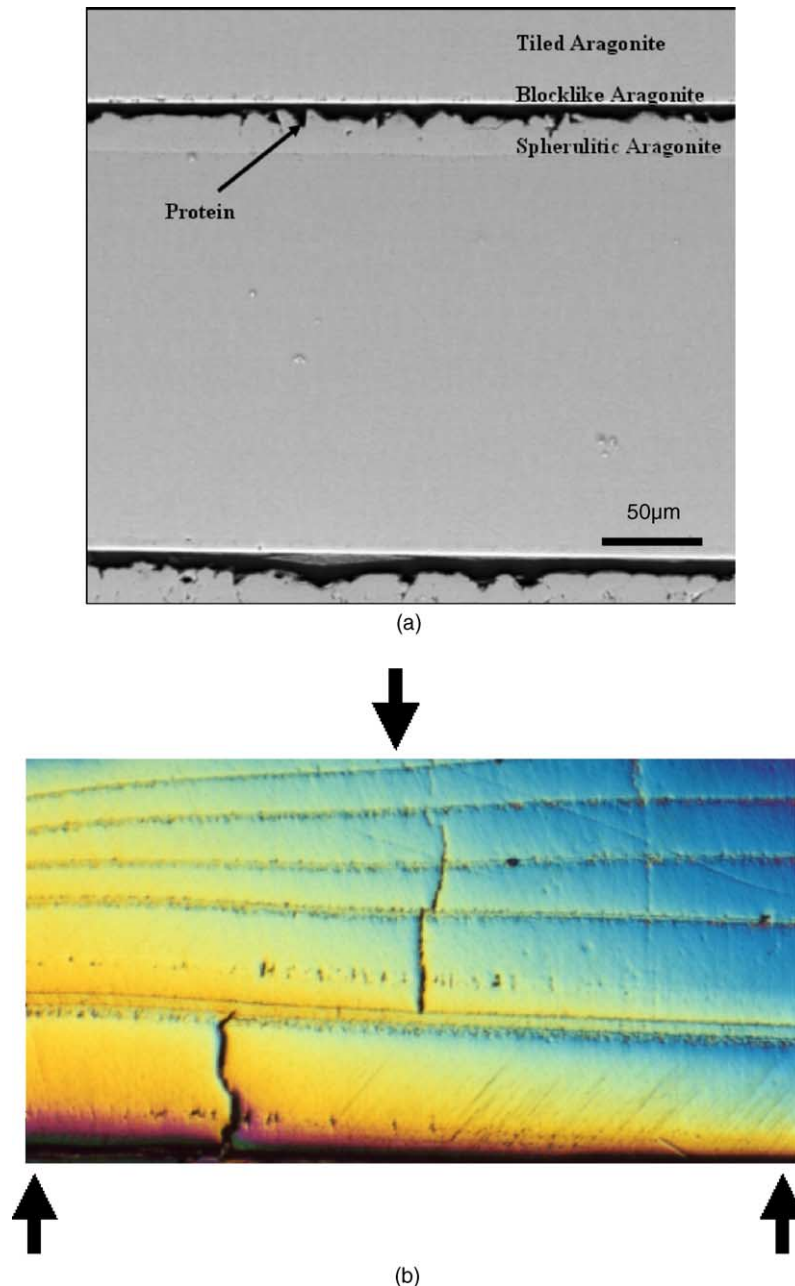
Fig. 4. (a) Detailed view of growth band (mesolayer) showing dark organic layers; first, interruption of aragonite formation (top of black organic layer) takes place; remineralization (bottom of organic layer) starts with irregular (spherulitic) layer and transitions to tiled aragonite; shell interior: bottom; (b) specimen subjected to flexure testing exhibiting crack deflection at mesolayers.

is clear evidence for faceting in the individual growing tiles in Fig. 8(b). This is consistent with differences between the propagation velocities V_a and V_b, which are the crystal growth velocities along directions X and Y, respectively (Fig. 5). Directions X and Y define the "basal" plane.

The stacking of tiles in Fig. 8(b) shows hexagons (with rounded edges) of decreasing size; their faces are parallel. Shown in Fig. 9 are schematic drawings of two growth sequences with a common c orientation: (a) random distribution of a and b orientations; (b) aligned a and b orientations. The situation more closely resembling Fig. 8 is the one in

Fig. 9(b); thus, one can conclude that all tiles along the same "Christmas tree" have the same crystallographic orientation.

Fig. 10 shows the sequence of growth, as it is thought to occur. First, a proteinaceous layer (possibly, the beta conformation of Addadi et al. [44]) is deposited. Then, a calcite layer (not shown in our sketch) is formed. The aragonite crystals nucleate and grow, with a characteristic spacing. They have the orthorhombic structure and it has been shown (e.g., Sarikaya [2]) that the c direction is perpendicular to the protein plane. In the absence of inhibiting proteins, this is the rapid growth direction. Addadi and Weiner [46] and Addadi
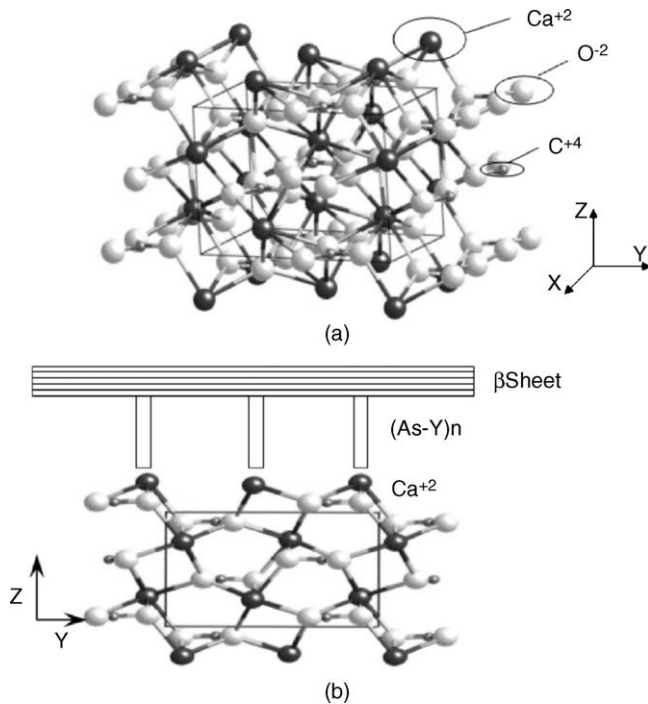
Fig. 5. Unit cell of aragonite: (a) perspective view; (b) normal view showing schematic position of (Asp-Y)$_n$ and β sheet. Notice protruding calcium ions on (0 0 1) face; black atoms: Ca; small black: carbon; gray atoms: oxygen (courtesy of K.S. Vecchio, UCSD).

et al. [44] demonstrated that there is stereoselective adsorption of proteins in the growth of calcite crystals; this results in a slowing down of growth in the *c* direction and completely alters the final shape of the crystals. This *c* direction corresponds to axis *Z* in Fig. 5. Addadi et al. [44] also showed that the (0 0 1) plane of calcite is the one that forms on the protein layer. The similarity between the two polymorphs (calcite and aragonite) of calcium carbonate is a strong indication that a
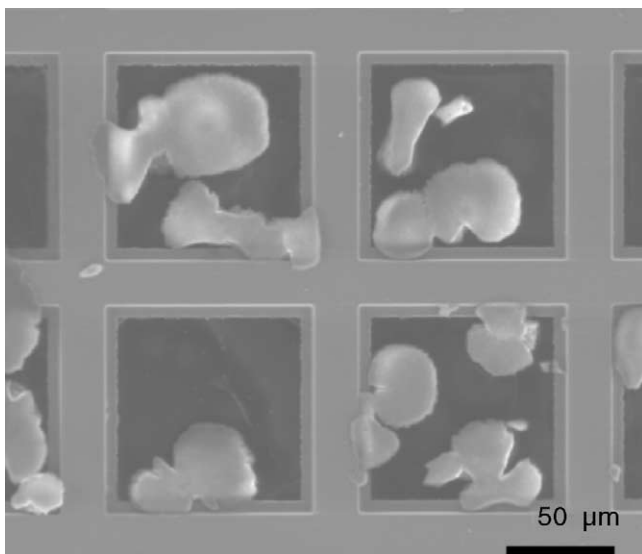
Fig. 6. Growth on 3 mm TEM disk after 3 days.
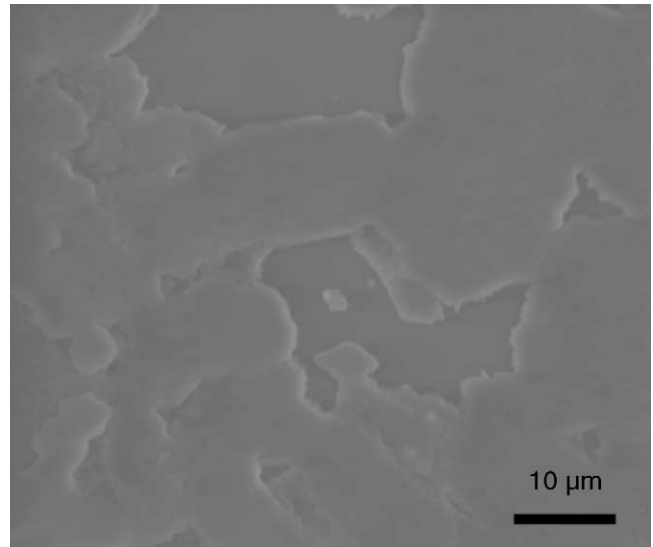
Fig. 7. Growth on 15 mm glass slide after 10 days.

similar mechanism might be operating. It is speculated that the host animal produces the proteins that arrest growth in the *c* direction in a periodic manner. Thus, the (0 0 1) growth is periodically arrested. New aragonite crystals nucleate at the growth surfaces, on the beta conformation layer. This occurs in parallel with lateral growth. In this fashion, successive "terraces" are formed and propagate. The resulting configuration is the "Christmas tree" reported by Fritz et al. [1]. The sequence shown in Fig. 10 can be described as:

(a) Random nucleation of aragonite crystals on protein.
(b) Lateral growth in (*a*, *b*) directions.
(c) Second growth spurt after deposition of beta sheet and nucleation.
(d) First aragonite plates are butted together while growth of second layer continues in *a* and *b* directions.
(e) Nucleation of third layer as second layer growth continues in *a* and *b* directions.

Recent results [21] indicate that mineralization in oyster shells is mediated by granulocytic hemocytes containing calcium carbonate. These granulocytes were observed in the regeneration of shell; a notch was introduced in the growth region. It should be pointed out that in oysters the mineral is calcite, and not aragonite. These results indicate that crystal nucleation on the organic sheets could involve hemocytes rather than direct nucleation from the mineral from the extrapallial fluid. Thus, this is still very much an area for open inquiry; Sarikaya [48] reports a central core along the "Christmas tree" trunk. This central core would be responsible for triggering lateral growth and would crystallographically link successive layers. Song et al. [49] report on mineral "bridges" between adjacent layers. Our observations in Fig. 8(b) indicate a light circle at the top of each tree. This would correspond to Sarikaya's core or to one of Song et al. [49] bridges. The configuration shown in Fig. 9(b) is consistent with the
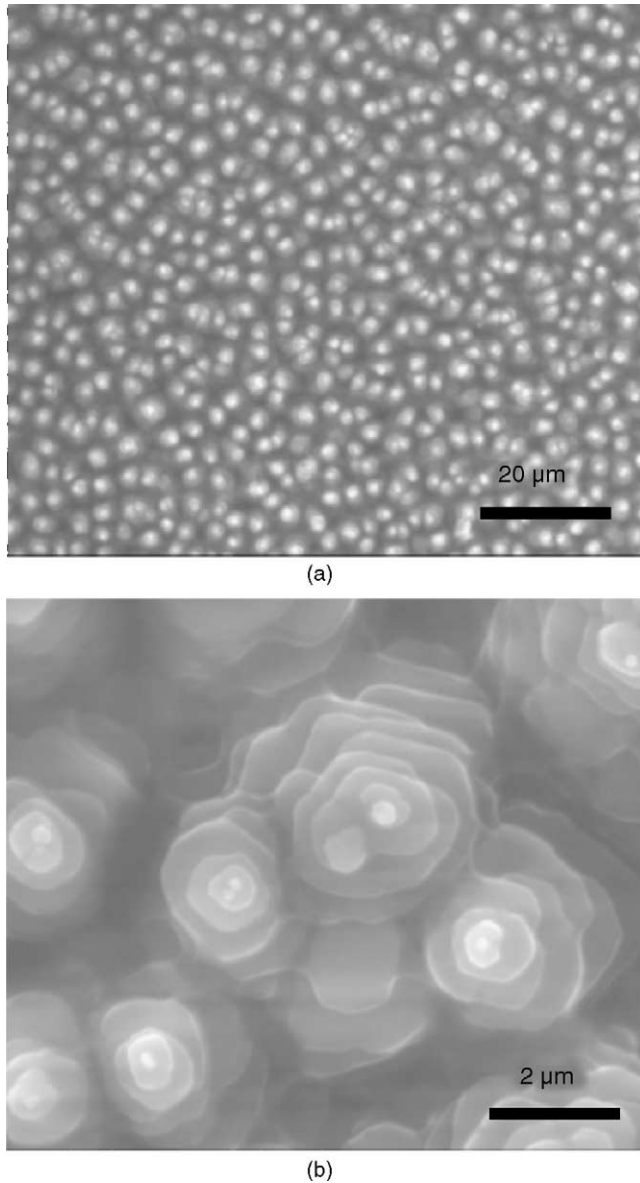
(a)

(b)

Fig. 8. Growth on 15 mm slide after 20 days; (a) low-magnification SEM; (b) high-magnification SEM.

mechanisms above. Our observations do not preclude the formation of a protein scaffold beyond the propagation front along a and b directions.

Fig. 11(a) shows a more detailed view of the growth process. Two adjacent "Christmas trees" are seen. Their spacing, d, determines the tile size. Two growth velocities are indicated: V_{ab}, representing growth velocity in the basal plane (we assume that $V_a = V_b$) and V_c, the growth in the c-axis direction. Since the growth in the c-axis direction is mediated by organic layer deposition, the real growth direction, V_c, is different from the apparent growth velocity, V_c'.

The apparent growth velocity (in the y direction) is:

$$V_c' = \frac{dy}{dt} = \frac{c}{t_N + t_G} \tag{1}$$

(a)

(b)
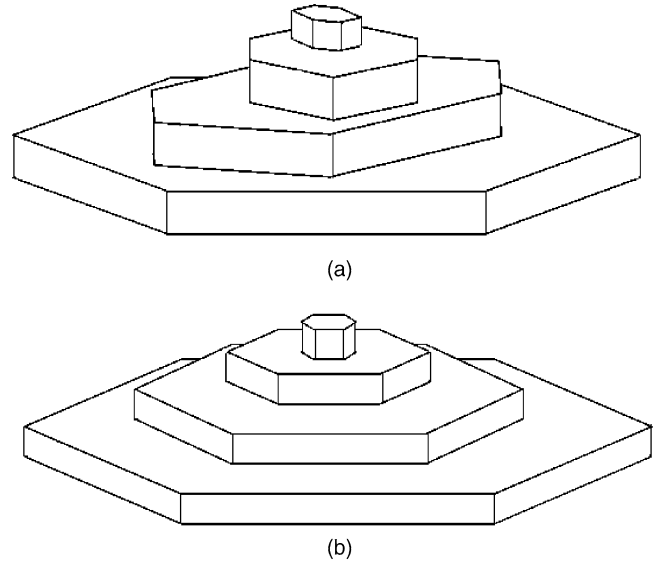
Fig. 9. Growth of successive layers of aragonite with common c axis: (a) random a and b orientations; (b) identical a and b orientations.

where c is the tile thickness ($=0.5 \, \mu m$). t_N and t_G are the nucleation and growth times, respectively. The velocity of growth in the (a, b) directions is:

$$V_{ab} = \frac{dx}{dt} = \frac{b}{t_N + t_G} \tag{2}$$

where b is the increment in tile diameter from layer to layer. The actual growth velocity is given by

$$V_c = \frac{c}{t_G} \tag{3}$$

The cone angle, α, is given by

$$\tan \alpha = \frac{V_{ab}}{V_c'} \tag{4}$$

It is possible to determine α from measurements made on the SEM micrographs of growing tiles (e.g., Fig. 8(c)). Measurements were made in several SEM micrographs and the results are plotted in Fig. 11(b). But the number of unknowns in Eqs. (1)–(4) still exceeds the number of variables; thus, two additional parameters are needed.

The experimental results obtained herein can serve to estimate the growth velocity, V_c'. Approximately 10 layers are observed in Fig. 8(b). This growth occurred from day 10 to 20. This corresponds to a growth rate of one tile per day, or 0.5 μm per day (5.78×10^{-12} m/s). It should be mentioned that the growth rate in abalone can vary significantly. Lapota et al. [51] report growth rates for red and green abalone. They find seasonal variation in growth velocity, averaging 36 mm per year (in length) for red abalone and 60 mm per year for green abalone. The thickness/diameter ratio for abalone is approximately 1/50. Thus, one can estimate a growth rate V_c' = 0.72 mm per year = 1.97 μm per day (2.3×10^{-11} m/s) (for a longitudinal growth velocity of 0.01 mm per day). Zaremba et al. [34] report maximum growth velocities of 5 μm per day,
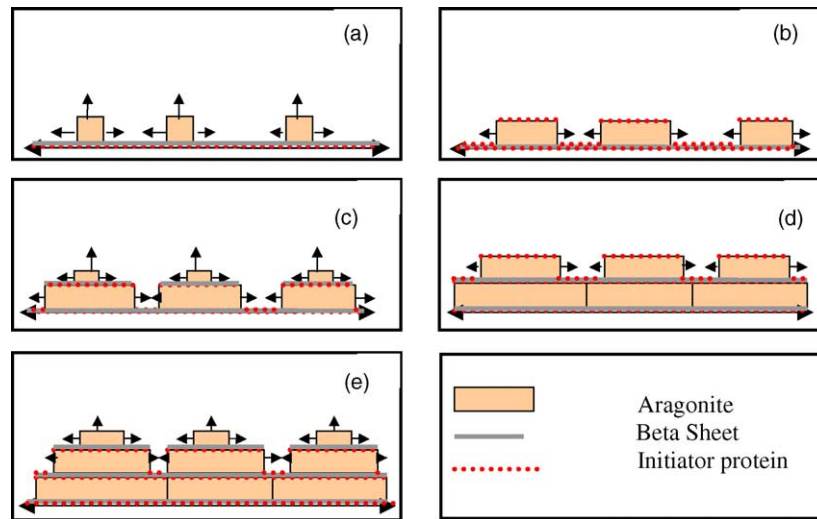
Fig. 10. Hypothetical growth mechanism with periodic injection of proteins arresting growth in *c*-direction: (a) nucleation of aragonite with *c*-axis perpendicular to protein layer; (b–e) growth with periodic protein regulation along (0 0 1) plane.
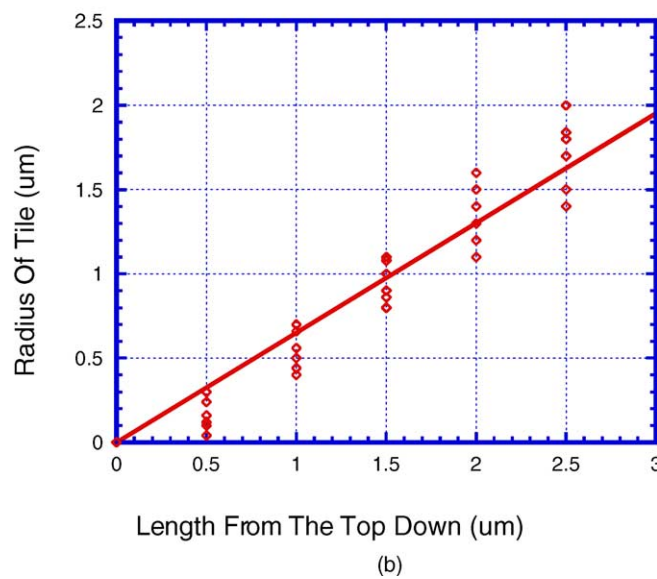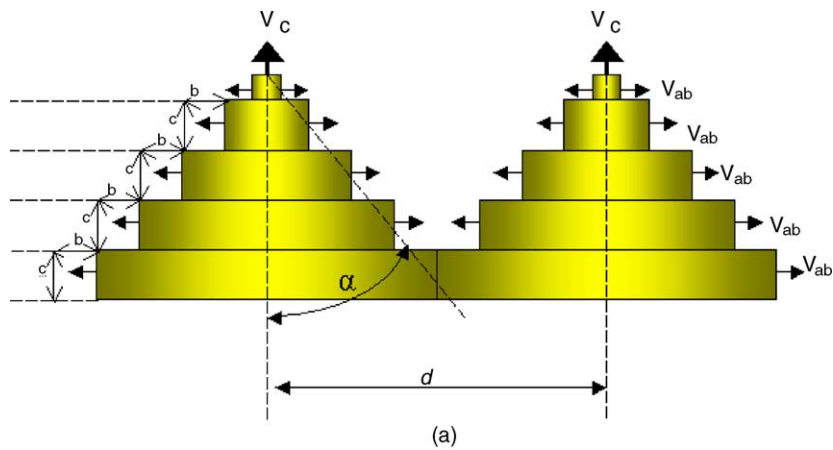

Fig. 11. (a) Schematic representation of the growth of two adjacent "Christmas trees" with velocities V_c and V_{ab} along crystallographic axes (a, b) and *c* marked. (b) Measured tile sizes, *d*, for successive layers.

corresponding to 5.78×10^{-11} m/s. Fritz et al. [1] report a growth rate of approximately 14 μm per day on a flat pearl. They report that this is ∼26 times the "normal" growth rate for pearls in bivalve mollusks, which would be 0.5 μm per day. This wide variation might be due to the fact that the growth of abalone is not coupled to tidal fluctuations; other mollusks show "growth bands" that correspond to tidal or daily cycles [50].

The growth along the c axis, V_c, in the absence of a periodic arrest mechanism such as the intercalation of organic layers in abalone can be estimated from coral growth. Coral is the aragonitic form of calcium carbonate and its growth occurs without protein mediation. This growth takes place in an environment that is fairly close to the one inside the shell in abalone. A growth velocity V_c estimated to be equal to 5 mm per year = 13.7 μm per day, was used in the calculations below [52]. This yields a growth velocity $V_c = 15 \times 10^{-11}$ m/s. For $V_c{}'$, the value from Lapota et al., which represents a good average, was used: 2.3×10^{-11} m/s [51]. The value of tan α = 2/3 is directly obtained from Fig. 11(b). By inserting these parameters into Eqs. (1)–(4), one obtains first estimates of the nucleation and growth times, t_N and t_G, respectively:

$$t_N = 16.4 \times 10^3 \, \text{s}, \quad t_G = 3.6 \times 10^3 \, \text{s}$$

Thus, the time during which the protein is being deposited to arrest and reinitiate the process of biomineralization is approximately equal to five times the growth time. It is also possible to estimate V_{ab}. From Eq. (1), one obtains $V_{ab} = 1.5 \times 10^{-11}$ m/s. The ratio V_c/V_{ab} is approximately 10. Direct observations from Fig. 1(b) of Thompson et al. [53] give a ratio of approximately 5. It was possible to estimate the angle α measured from Fig. 3 of Fritz et al. [1], which shows Christmas trees. Surprisingly, it is significantly lower (α = 17°) than the one measured here (α = 34°). The possible explanation is that the observation direction used by Fritz et al. [1] is oblique. Indeed, the SEM observation was carried out at an oblique angle to the c axis of the tree (tree axis); by making the appropriate correction, one arrives at the required difference.

It should also be noticed that the thickness of mesolayers is consistent with an annual pattern of growth arrest. Annual growth rate can be obtained for the shells and is approximately 0.6 mm. This quantity is approximately the double of the mesolayer thickness. Thus, the growth rate with an annual arrest and the formation of a thick protein layer would reduce the annual growth from 0.6 to 0.3 mm.

4.2. Tile size dependence on animal size

In order to see whether the tile size was dependent on animal size, a 100 mm green abalone were obtained from Dr. Leighton. A 200 mm diameter red abalone was also available. Fig. 12 shows fracture surfaces for three sizes. The tiles are virtually undistinguishable. They have the same 0.5 μm thickness and 10 μm diameter. The fracture occurs by pullout of the platelets.
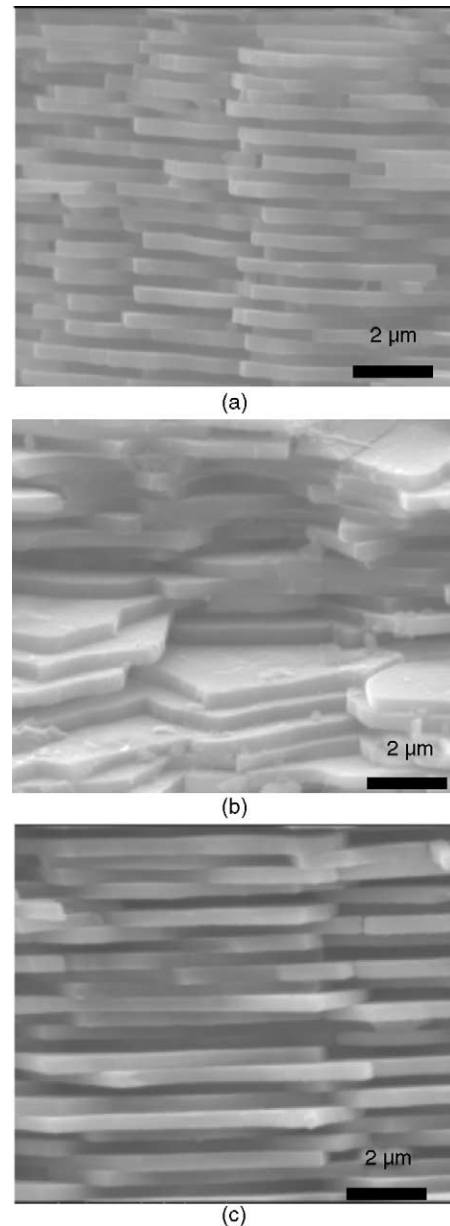

(a)

(b)

(c)

Fig. 12. Tile configuration (on fractured surface) for shells having approximately 10, 100, and 200 mm length.

4.3. Configuration of proteinaceous layer

Another interesting and intriguing aspect that was investigated was the distribution of the proteinaceous layer around the aragonite tiles. If the mechanism represented in Figs. 10 and 11 is correct, the proteins are deposited along the (0 0 1) faces. This was indeed observed. We found only scant evidence for the protein layer along the lateral surfaces of the tiles. Fig. 13(a) shows this in a clear manner. It is a backscattered SEM micrograph. The organic layer, that has a lower Z, shows up as a dark band. This organic layer is very regular. It should be noted that no mineral bridges between adjacent layers [48] are observed. Neither is the rugosity
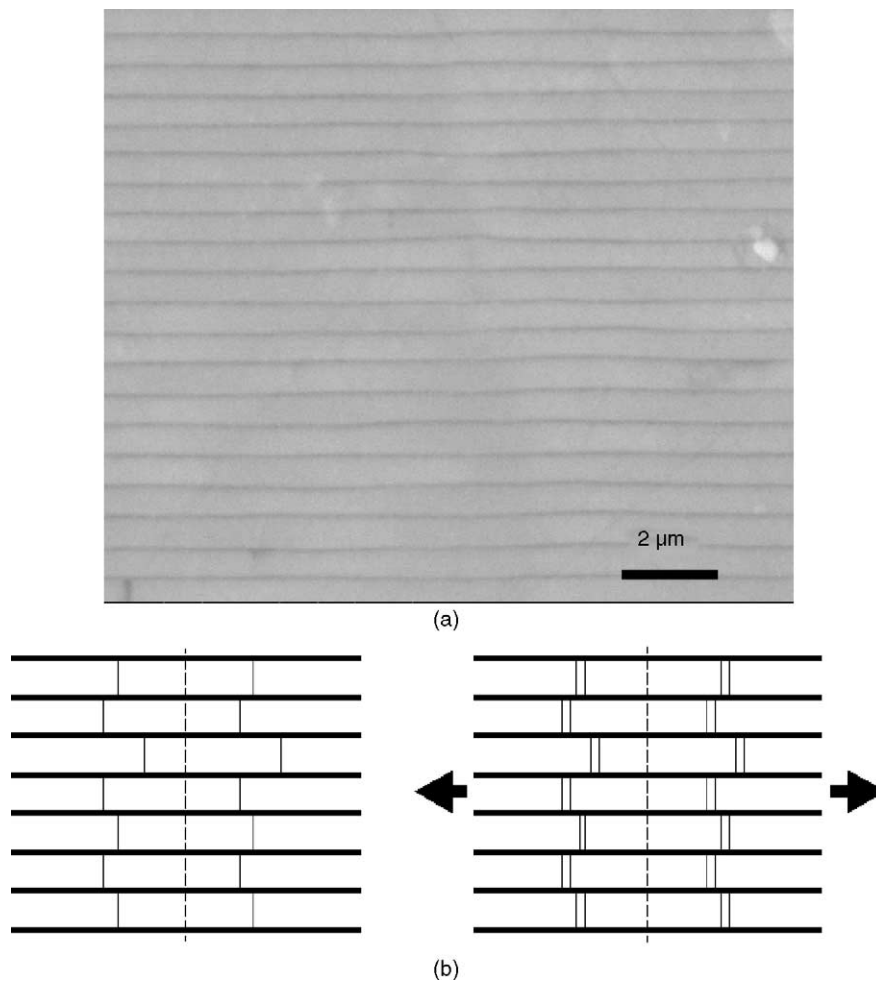
Fig. 13. (a) SEM of cross-section of abalone, showing protein layer (darker regions) and its virtual absence where tiles on same plane join; (b) schematic drawing of stacking of abalone tiles and their separation under tension.

reported by Evans et al. [32] and Wang et al. [33] seen in this micrograph. It is possible that the shell they used was desiccated and that meandering cracks formed along the interface, giving it the appearance of inherent rugosity. Fresh shells, with hydrated organic layers, would have deformed differently. Indeed, Jackson et al. [25] points out the effect of shell hydration on the mechanical properties. Similar observations were made in different shells. It can be concluded that the organic layer is remarkably regular and that it forms primarily along the (0 0 1) plane of aragonite. There does not seem to be such a regular protein layer along the lateral surfaces of the tiles.

Fig. 13(b) shows a schematic representation of tile stacking with the organic layer marked by a thicker line. Upon being subjected to tension parallel to the tile plane, the tiles slide, rather than fracture. The absence of organic glue along the lateral surfaces of the tiles, where they abut, contributes to the sliding mechanism. If the edges were glued, there would be a greater tendency for fracture of the individual tiles, with less energy absorption. Fig. 14(a) shows a specimen subjected to tension in such a direction. The dark rectangular features

are gaps that opened between tiles during tension. The tiles slide past each other rather than fracturing. This sliding has been identified by Sarikaya [2] as a toughening mechanism and documented by Evans et al. [32].

The overlap of tiles was estimated from direct measurements along fracture surfaces, as shown in Fig. 14. The tiles are pulled out and the step height corresponds to the overlap. It was also measured from Fig. 7(e) of Wang et al. [33] and Fig. 2(b) of Evans et al. [32]. The following average values were obtained

Current work: fracture 1	0.57 μm
Current work: fracture 2	0.85 μm
Wang et al. [33]	1.07 μm
Evans et al. [32]	1.35 μm

It is possible that the lower readings obtained in the current research are due to more frequent fractures caused by shell desiccation.
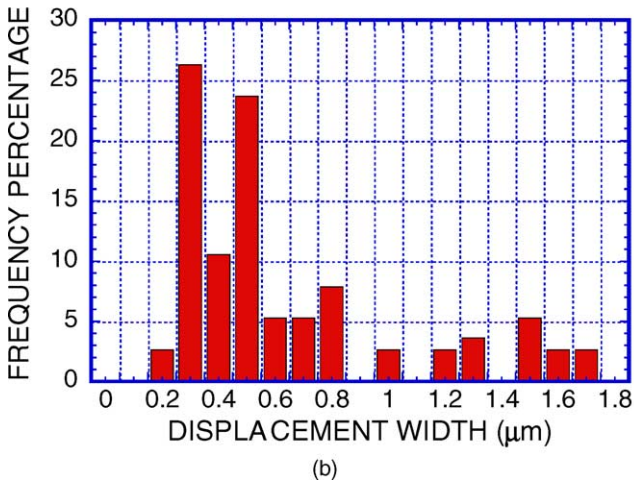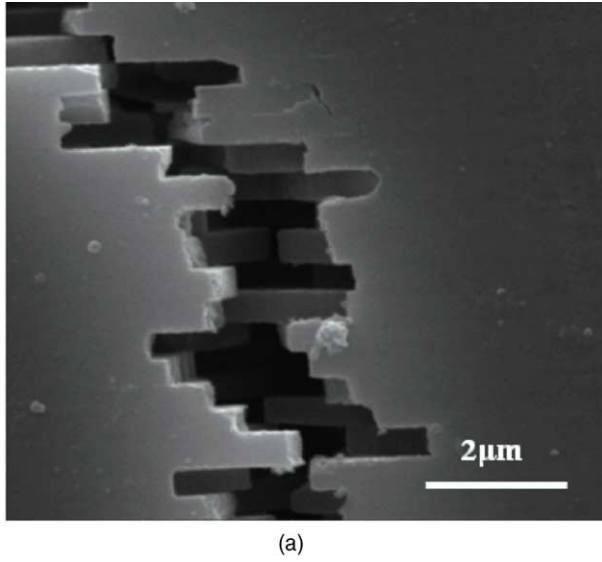
(a)

(b)

Fig. 14. (a) SEM photography of polished cross-section after plastic deformation under tension; notice fracture by tile "pullout"; (b) plot showing distribution of step lengths.

Fig. 15 shows the schematic representation of tile overlap. In Fig. 15(a) three tiles are shown, subjected to tension. A simpler two-dimensional representation is shown in Fig. 15(b). It is interesting to note that the tiles are designed in such a manner that sliding (pull out) occurs before tensile failure. Taking the equilibrium of forces in Fig. 15(c):

$$F_1 = F_2 + F_3 \tag{5}$$

In terms of tensile stress on tile, σ_t, and shear stress on organic interfaces, τ_s:

$$\sigma_t t = 2\tau_s d \tag{6}$$

Assuming that $d = 1\,\mu m$ and $t = 0.5\,\mu m$:

$$\frac{\sigma_t}{\tau_s} = \frac{2d}{t} = 4 \tag{7}$$

Thus, the tensile strength of the ceramic should be, at least, equal to four times the shear strength of the organic layer.
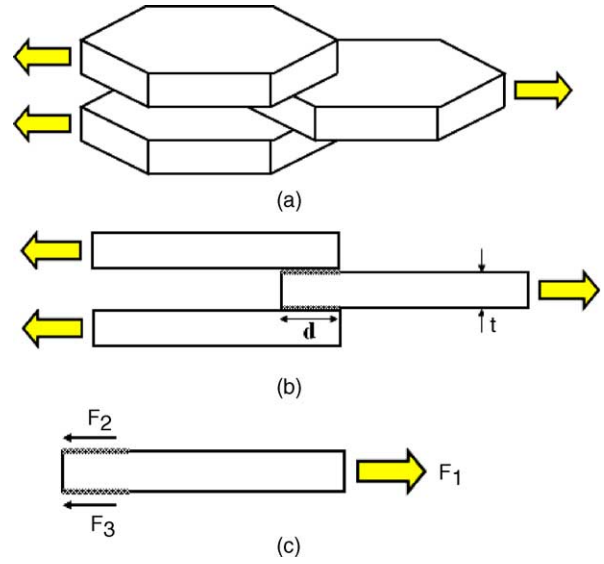

Fig. 15. Schematic diagram showing pull-out of overlapping tile layers; (a) tri-dimensional view; (b) two-dimensional view; (c) force diagram.

The mechanical response of these two constituents can be measured and preliminary data are available for the shear strength of the organic glue. Menig et al. [22] carried out shear tests, from which the shear strength can be expressed as:

$$\tau_s = \tau_0 + k\gamma \tag{8}$$

where $\tau_0 = 10\,MPa$ and $k = 1000$. γ is the shear strain within the organic layer, obtained from the overall strain by multiplying it by 20, the ratio between aragonite and organic component fractions. Thus, there is considerable viscoplasticity, and the strength of the layer increases with shear strain. This corresponds to the stretching and deconvolution of the chains.

Fig. 16 shows the tensile strength of the aragonite phase as a function of crack size. The fracture toughness was taken as $1\,MPam^{1/2}$. It can be seen that, if one considers the strength
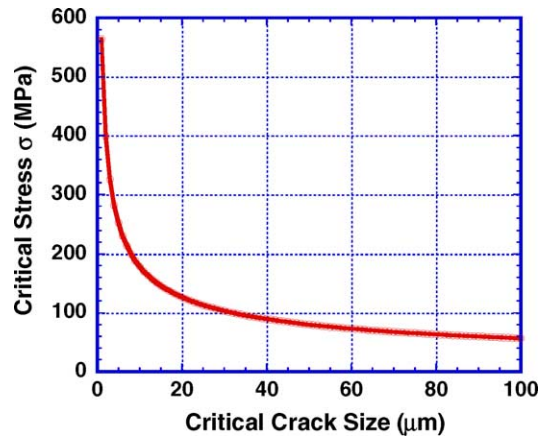

Fig. 16. Critical stress as a function of flaw size for aragonite [$K_{IC} = 1\,MPam^{1/2}$].

limited by flaw size, that it increases from values of ~50 MPa for large flaws to 250 MPa for a flaw the size of a tile (10 μm). The strength of tiles increases with decreasing size, and one can safely assume that it is higher than 250 MPa, for the given size. Thus, the values of tensile strength obtained by Menig et al. [22] (180 MPa from flexure tests) and Wang et al. [33] (110 MPa) are explained by the viscoplastic flow of the organic layer, starting at 10 MPa and proceeding through gradual increase due to the viscoplastic response, until separation occurs.

4.4. Environmental dependence of shell growth

After 6 months of controlled culturing of the abalone, changes in growth patterns were observed. A change from tiled aragonite growth to a block-like structure occurred due to environmental changes in the circulating seawater of the holding tank. Su et al. [41] identified the block-like structure formed in the growth bands as aragonite. These changes, in contrast to specimens currently raised in constantly flowing seawater within our facilities at Scripps Institute of Oceanography, can be seen in Fig. 17. It is estimated that the switch from aragonite growth to calcite growth occurred 6 months before the examination presented in Fig. 17. This would indicate that the calcite grew an average distance of 40 μm over the span of 6 months along the vertical plane, or 0.22 μm per day. It should be noted that the sample was brittle in comparison to previous samples that did not present this calcitic mesolayer. The cross-sectional view shown in Fig. 17 reveals several columnar bands extending across the horizontal planes of the shell. It is believed that these bands represent fluctuations in the physical status of the animal.

This transition from tiled to columnar morphology is also shown in the bottom of Fig. 18(a), which represents a fracture surface. One of the growth bands (mesolayers) discussed in Section 3 (Fig. 4(a)) is also shown in the same figure. One can see the tiled, block-like, and spherulitic aragonite (as identified by Su et al. [41]). It was possible to see the block-
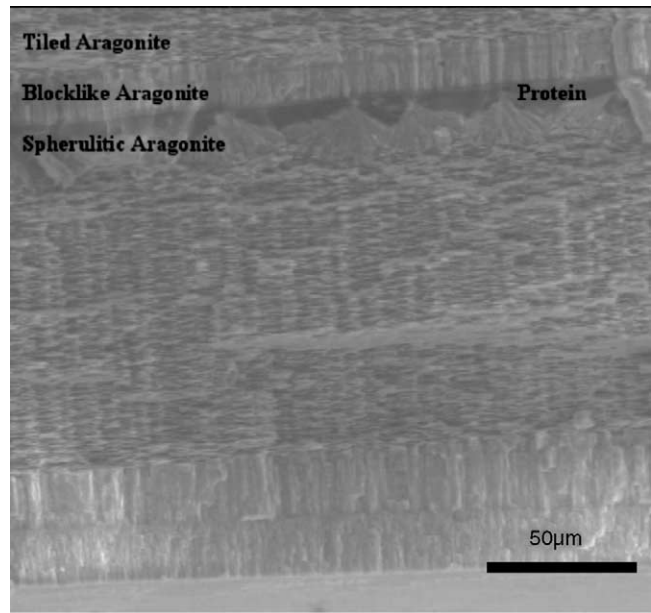
(a)
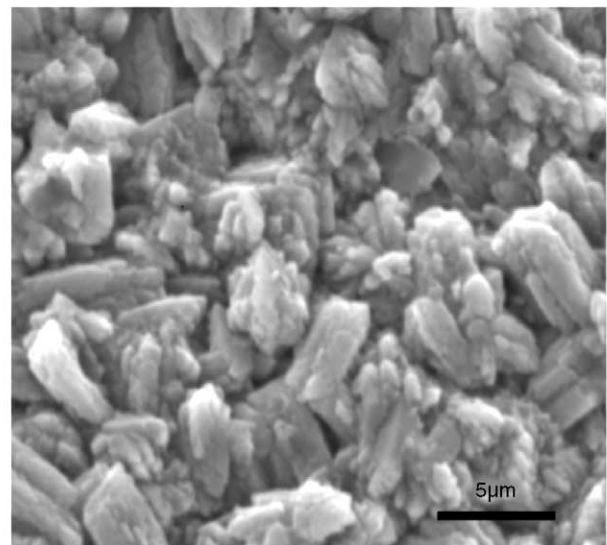
(b)

Fig. 18. (a) SEM micrograph of growth surface showing three morphologies of aragonite: tiled, block, and spherulitic; (b) top view block-like aragonite structure observed in "flat pearl" edge.

like growth of crystals along the edges of the glass slides. This structure is shown in Fig. 18 (b). It consists of columnar grains with a favored growth axis. Thus, it is concluded that the block-like or spherulitic growth takes place when arrestor proteins are not injected into the growth areas. In well-regulated growth conditions, the mechanism depicted in Fig. 11 operates.

5. Conclusions

Biologically engineered synthesis processes will very likely guide some of the most revolutionary future approaches
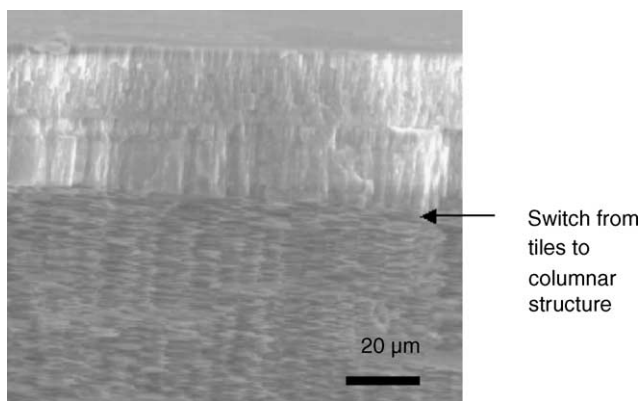

Fig. 17. SEM micrograph of cross-sectional fracture surface of green abalone shell that has been cultured with environmentally-controlled variations in seawater content and feeding.

to the synthesis of a next generation of structural and electronic materials. In spite of this, even the simplest bio-induced structures of interest are currently impossible to synthesize. A detailed understanding of the growth and structure is essential, if these processes will be bioduplicated and biomimicked in the future. For the specific case of the abalone shell, an exploratory investigation has been carried out to elucidate some of the mechanical property results obtained earlier [22]. Its growth and structure was characterized. The following are conclusions that have a bearing on the mechanical response of these shells:

(a) The growth proceeds by the sequential deposition of aragonite and organic layer along the c-axis orientation. The Christmas tree pattern was confirmed and an analytical model for growth is proposed. The velocities of growth along the basal (a and b) and c directions are obtained and a nucleation time for each layer is inferred. The following velocities and times are calculated (it should be mentioned that these values can vary considerably):

$$V_c = 15 \times 10^{-11} \text{m/s} \quad V_c{}' = 2.3 \times 10^{-11} \text{m/s}$$

$$V_{ab} = 1.5 \times 10^{-11} \text{m/s} \quad t_N = 16.4 \times 10^3 \text{s}$$

$$t_G = 3.6 \times 10^3 \text{s}$$

(b) The organic layer attaches itself to the basal planes of aragonite, so that there is virtually no organic material where platelets abut. This is consistent with the stereoselective attachment of proteins to the basal planes.

(c) It is proposed that the animal injects, periodically, the organic material that arrests the growth in the c direction. If this growth were not arrested, long needles would form that would penetrate the extrapallial space and cause trauma to the epithelium. Based on this, a simple mechanism for growth is proposed.

(d) Growth of aragonite is periodically (seasonally) arrested in abalone. Mesolayers (or heterolayers [34]) of organic material with the thickness of approximately 10–20 μm are periodically formed as a result of seasonal fluctuations. They play a prominent role in the mechanical strength and are a determining factor in plastic microbuckling (kinking).

(e) A mechanism for tensile deformation of the abalone is proposed, based on viscoplastic shear of the organic layer.

References

[1] M. Fritz, A.M. Belcher, M. Radmacher, D.A. Walters, P.K. Hansma, G.D. Strucky, D.E. Morse, Nature 49 (1994) 371.
[2] M. Sarikaya, Microsc. Res. Technique 27 (1994) 360.
[3] A.V. Srinivasan, G.K. Haritos, F.L. Hedberg, Appl. Mech. Rev. 44 (1991) 463.
[4] J.F.V. Vincent, Structural Biomaterials, Princeton University Press, Princeton, NJ, 1991.
[5] E. Baer, A. Hiltner, R.J. Morgan, Phy. Today Oct. (1992) 60.
[6] A.H. Heuer, D.J. Fink, V.J. Laraia, J.L. Arias, P.D. Calvert, K. Kendall, G.L. Messing, J. Blackwell, P.C. Rieke, D.H. Thompson, A.P. Wheeler, A. Veis, A.I. Caplan, Science 255 (1992) 1098.
[7] J.V. Laraia, A.H. Heuer, J. Am. Ceram. Soc. 72 (1989) 2177.
[8] J.F.V. Vincent, P. Owers, J. Zool. (A) (1986).
[9] G. Mayer, M. Sarikaya, Exp. Mech. 42 (2002) 395.
[10] L.F. Kuhn-Spearing, H. Kessler, E. Chateau, R. Ballarin, A.H. Heuer, J. Mater. Sci. 31 (1996) 6583.
[11] M. Sarikaya, J.A. Aksay, in: S. Case (Ed.), Results and problems in cell differentiation in biopolymers, Springer-Verlag, Amsterdam, 1992, p. 1.
[12] M. Sarikaya, K.E. Gunnison, M. Yasrebi, J.A. Aksay, Mater. Res. Soc. 174 (1990) 109.
[13] J.D. Currey, A.J. Kohn, J. Mater. Sci. 11 (1976) 1614.
[14] J.D. Currey, Proc. Roy. Soc. London B 196 (1977) 443.
[15] G. Nicolis, I. Prigogine, Self-organization and nonequilibrium thermodynamics: from dissipative structures to order through fluctuations, Wiley, New York, 1977.
[16] G. Whitesides, Mater. Res. Bull. Jpn. (2002) 56.
[17] H.A. Lowenstam, S. Weiner, On Biomineralization, Oxford University Press, New York, 1989.
[18] K. Simkiss, K.M. Wilbur, Biomineralization, Academic Press, 1989.
[19] E. Bauerlein (Ed.), Biomineralization, Wiley-Interscience, Weinheim, Germany, 2000.
[20] S. Mann, Biomineralization, Oxford, 2001.
[21] A.S. Mount, A.P. Wheeler, R.P. Paradkar, D. Snider, Science 304 (2004) 297.
[22] R. Menig, M.H. Meyers, M.A. Meyers, K.S. Vecchio, Acta Mater. 48 (2000) 2383.
[23] R. Menig, M.H. Meyers, M.A. Meyers, K.S. Vecchio, Mater. Sci. Eng. A297 (2001) 203.
[24] M.A. Meyers, K.K. Chawla, Mechanical Behavior of Materials, Prentice Hall Inc., Saddle River, NJ, 1999, p. 41.
[25] A.P. Jackson, J.F.V. Vincent, R.M. Turner, Proc. Roy. Soc. B London (Biol.) B234 (1988) 415.
[26] W. Weibull, J. Appl. Mech. 18 (1951) 293.
[27] A.G. Evans, W.F. Adler, Acta Met. 26 (1977) 725.
[28] A.S. Argon, Fracture of Composites. Treatise of Materials Science and Technology, Academic Press, New York, 1972, p. 1.
[29] B. Budiansky, Comp. Struct. 16 (1983) 3.
[30] N.A. Fleck, L. Deng, B. Budiansky, J. Appl. Mech. 62 (1995) 329.
[31] P.M. Jelf, N.A. Fleck, J. Comp. Mater. 26 (1992) 18.
[32] A.G. Evans, Z. Suo, R.Z. Wang, I.A. Aksay, M.Y. He, J.W. Hutchinson, J. Mater. Res. Soc. 16 (2001) 2475.
[33] R.Z. Wang, Z. Suo, A.G. Evans, N. Yao, I.A. Aksay, J. Mater. Res. Soc. 16 (2001) 2485.

[34] C.M. Zaremba, A.M. Belcher, M. Fritz, Y. Li, S. Mann, P.K. Hansma, D.E. Morse, Chem. Mater. 8 (1996) 679.

[35] A.M. Belcher, Ph.D. Thesis, University of California, Santa Barbara, 1996.

[36] A.M. Belcher, X.H. Wu, R.J. Christensen, P.K. Hansma, G.D. Stucky, D.E. Morse, Nature 38 (1996) 156.

[37] X. Shen, A.M. Belcher, P.K. Hansma, G.D.S. Stucky, D.E. Morse, J. Biol. Chem. 272 (1997) 32472.

[38] A.M. Belcher, P.K. Hansma, G.D. Stucky, D.E. Morse, Acta Mater. 46 (1997) 733.

[39] A.M. Belcher, E.E. Gooch, in: E. Bauerlein (Ed.), Biomineralization, Wiley-VCH, Weinheim, 2000, p. 221.

[40] M. Fritz, D.E. Morse, Col. Int. Sci. 3 (1998) 55;
X. Su, A.M. Belcher, C.M. Zaremba, D.E. Morse, G.D. Stucky, A.H. Heuer, Chem. Mater. 14 (2002) 3106.

[41] X. Su, A.M. Belcher, C.M. Zaremba, D.E. Morse, G.D. Stucky, A.H. Heuer, Chem. Mater. 14 (2002) 3106.

[42] H. Nakahara, G. Bevelander, M. Kakei, Venus 41 (1982) 33.

[43] S. Weiner, Am. Zool. 24 (1984) 945.

[44] L. Addadi, J. Moradian, E. Shay, N.G. Maroudas, S. Weiner, Proc. Natl. Acad. Sci. U.S.A. 84 (1987) 2732.

[45] S. Weiner, W. Traub, FEBS Letts. 111 (1982) 311.

[46] L. Addadi, S. Weiner, Proc. Natl. Acad. Sci. U.S.A. 82 (1985) 4110.

[47] S. Weiner, Cal. Tissue Int. 29 (1979) 163.

[48] M. Sarikaya, Personal Communication, 1997.

[49] F. Song, A.K. Soh, Y.L. Bai, Biomaterials 24 (2003) 3623.

[50] D.J. Crisp, in: R.E. Crick (Ed.), Origin, Evolution, and Modern Aspects of Biomineralization in Plants and Animals, Plenum Press, New York, 1986, p. 103.

[51] D. Lapota, G. Rosen, J. Chock, C.H. Liu, J. Shellfish Res. 19 (2000) 431.

[52] http://geology.uprm.edu/Morelock/GEOLOCN_/rfbuild.htmin.

[53] J.B. Thompson, G.T. Palczi, H.K. Kindt, M. Michenfelder, B.L. Smith, G. Stucky, D.E. Morse, P.K. Hansma, Biophys. J. 79 (2000) 3307.